

An Integrated Design Procedure for High Frequency AC Inductors for Inverters

Parikshith B.C, Anusyutha Krishnan and Vinod John

Department of Electrical Engineering
Indian Institute of Science,
Bangalore 560012, India
Email: pariks@ee.iisc.ernet.in

Amith Karanth

Department of Electrical Engineering and IT
Technische Universität Darmstadt,
64283 Darmstadt, Germany
Email: amith.karanth@stud.tu-darmstadt.de

Abstract—Inductors are important energy storage elements that are used as filters in switching power converters. The operating efficiency of power inductors depend on the initial design choices and they remain as one of the most inefficient elements in a power converter. The focus of this paper is to explore the inductor design procedure from the point of efficiency and operating temperature. A modified form of the area product approach is used as starting point for the inductor design. The equations which estimate the power loss in core and copper winding are described. The surface temperature of the inductor is modelled using heat transfer equations for radiation and natural convection. All design assumptions are verified by actual experimental data and results show a good match with the analysis.

Keywords: Bessel functions, Eddy currents, Loss measurement, Magnetic circuits, Pulse width modulated inverters, Temperature measurement

I. INTRODUCTION

Inductors are important energy storage elements that are used as filters in switching power converters. The shift towards higher switching frequencies at higher power densities in power converters has had a negative effect on inductor efficiency and operating temperature. The operating efficiency of power inductors depend on the initial design choices and once manufactured, the designer has no control on the performance or efficiency. Hence poorly designed inductors remain one of the most inefficient elements in a power converter. The principal cause for this inefficiency is that the inductor design principles are inherently complicated with many design variables which have to be simultaneously tuned for high frequency high power operation.

The design process for low frequency (50Hz-60Hz) inductors used for uncontrolled rectifiers or thyristor controlled applications is quite established. The same design principles cannot be applied in case of high frequency AC inductors for inverter applications. Although there is considerable literature related to high frequency inductor design issues, they are mostly geared towards switched mode power supply applications where the inductor current is primarily DC. AC inductors for inverter applications need to have tight parameter tolerances due to the requirement for well defined resonance frequency. Furthermore, grid interactive applications can have a design life of the order of 20-30 years requiring accurate

prediction of operating temperature for system life consideration.

Most of the existing literature on inductor design feature some kind of iterative procedure to optimize important inductor parameters such as core size, window utilization, power loss, temperature rise etc. The reason for this iterative approach is that inductor design is a complicated process with many electrical and material dependencies which cannot be satisfied to get an optimal design in a single pass. The design conclusions will also vary widely depending on the initial assumptions on current density, flux density, power loss and temperature model. This also means that each approach can give a different inductor specification for the same inductor rating.

An iterative design procedure based on a volume optimized ferrite core database is discussed by [1]. A ferrite core database is generated and design parameters such as current density, flux density, total power loss and thermal resistance are estimated based on a specific core dimension, called the characteristic dimension. The design process then uses this database for a specific inductor design. The design is fast since most of the relevant parameters are already available via the core database. This procedure focuses on matching the required inductor stored energy to the actual stored energy of the selected core.

It is also possible to fix the the total power loss of the inductor early in the design, as in [2] which proposes a non-saturated thermally limited design. The core size is selected based on total volt-ampere rating. The total heat dissipation capability of the core is then estimated based on largest core dimension assuming natural convection. Copper loss and core loss are assumed to equal to half the total power loss. The focus is on matching the expected power loss by choosing the number of turns and wire diameter. The design is tweaked to get the required inductance by varying the air gap.

The reverse procedure is adopted by [3] -the parameters which decide the inductance, such as number of turns, air gap, flux density etc are fixed initially. The power loss and temperature rise for these setting are calculated and the iterative procedure is focused on matching the temperature limit with the estimated temperature. There are other variations such as [4] which follows an iterative process concentrated on maximizing the window utilization factor by adding or

removing turns while maintaining the required inductance. The effect of fringing of the magnetic flux at air gaps is taken into account by [6].

The specific contribution of this paper is to present a simplified iterative inductor design procedure by including the important design principles from [1]- [6]. The focus is on high current high frequency filter inductors where there are significant challenges in maintaining lower operating temperatures. Another contribution is the application of heat transfer equations to improve the accuracy of estimated surface temperature.

Section II discusses the steps to design an AC inductor. The familiar area product equation is modified to increase the accuracy between design and construction. A new approach for selecting the air gap and number of turns is proposed by incorporating the effect of fringing of magnetic flux at air gap. Section III describes the equations to calculate the power loss in the core and copper winding. Heat transfer equations are used to iteratively estimate the surface temperature of the inductor for natural convection in Section IV. Experimental results to validate the analysis are presented in Section V.

II. DESIGN OF AC INDUCTOR

The typical configuration of a three phase grid connected inverter with inductive filter is shown in Fig 1. However, in recent years there has been significant interest in higher order filters, especially LCL filters, to meet the grid interconnection standards at significantly smaller size and cost. Higher order filters can lead to lower current ripple at the grid side [5]. The typical parameter ratings assuming a power level of 10 kVA are shown in Table I. From the table, $i_{g(sw)}$ is the switching frequency current ripple at the grid-interconnection point. This is specified for different converter ratings and grid conditions by standards like IEEE 519-1992 and IEEE 1547. This parameter has a significant impact on the final design ratings and operating efficiency of the inductor.

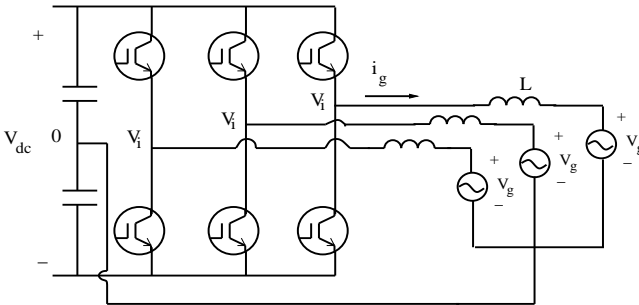


Fig. 1. Three phase grid connected inverter with L filter

TABLE I
TYPICAL CONVERTER RATINGS

KVA	V_{base}	I_{base}	$i_{g(sw)}$	f_1	f_{sw}	V_{dc}
kVA	V	A	A	Hz	kHz	V
10	239.6	13.91	0.042	50	10	861

The product of core cross-section area and window area in an inductor is a measure of the energy handling capability of the inductor. The area product equation is a good starting point for design since it relates the electrical design inputs with material and spatial constraints. The area product equation for an inductor handling AC is given by [6]

$$A_p = \frac{V_f I_f}{k_f k_u f B_m J_m} \quad (1)$$

where V_f is the voltage across the inductor at frequency f , I_f is the current through the inductor, k_f is the form factor ($k_f=4.44$ for sinusoidal waves), k_u is the core window utilization factor, B_m is the maximum allowable flux density in the core before saturation and J_m is the current density limit in the conductors to prevent overheating of the winding.

The maximum flux density B_m depends on the core material selected. The flux density limits of some magnetic materials used for high frequency inductors is detailed in Table II. The maximum flux density limit has significant implications on the size of the inductor, i.e. lesser the flux density, bigger the inductor to avoid saturation of the core for the same peak current. The window utilization factor k_u depends on the size, type of the copper winding, core shape and type of bobbin [6]. The current density limit J_m is decided by the constraint on the maximum operating temperature of the winding. The conductor size in turn depends on J_m .

$$a_{cu} = \frac{I_{rms}}{J_m} \quad (2)$$

where a_{cu} is the cross section of the copper winding carrying a current I_{rms} when the current density is set at J_m .

TABLE II
MAXIMUM FLUX DENSITY LIMIT

Material	B_m (T)
Ferrite	0.4
Amorphous	1.56
Powder	1.6

After selection of a suitable core material, the next step is to choose the appropriate core size from the manufacturer data sheets. Any selected core must have an area product at least equal to A_p to satisfy the electrical requirements. After selecting the core, number of copper turns and the length of the air gap in the magnetic path for the required inductance should be fixed. If the core material selected has stable permeability with respect to temperature, flux density, and air gap, such as Ferrites then linear magnetic circuit equations are sufficient to accurately determine the inductance. The linear magnetic circuit equations are

$$L = \frac{N^2}{\mathcal{R}_t} \quad (3)$$

$$B_m = \frac{N I_p}{A_e \mathcal{R}_t} \quad (4)$$

where N is the total number of copper winding turns, I_p is the peak current, A_e is the core cross section area and \mathcal{R}_t is

the total reluctance of the magnetic path, including reluctance of air gap if present. (3) and (4) show that L and B_m are functions of N and l_g .

$$L = f(N, l_g) \quad (5)$$

$$B_m = g(N, l_g) \quad (6)$$

where l_g is the total length of the air gap in the magnetic path.

If an air gap is introduced in the magnetic path, the fringing of the flux at the gap must be modelled accurately to estimate the inductance and prevent saturation. The fringing flux depends on the length of the air gap, shape and geometry of the core at the gap, and shape and location of winding and other objects such as clamps, brackets etc. Fringing effect becomes more noticeable as the air gap increases and simultaneously the air gap reluctance becomes more difficult to estimate. It is possible to model this fringing flux with electromagnetic FEM simulation, but higher accuracy requires large computation times. The challenge is to estimate air gap reluctance analytically by a closed-form solution using the dimensions of the core and/or air gap as the input. There are several publications that have tried to model the magnetic flux patterns at the air gap [4], [7]- [8]. A modified form of [4] has been used here since it provides a good balance between simplicity and accuracy.

The fringing at the air gap is modelled as increase in area of the air gap cross section, and this increase is in terms of l_g . The air gap reluctance \mathcal{R}_g for an air gap of l_g and core cross section area of $a_e = f \times d$ is given by

$$\mathcal{R}_g = \frac{l_g}{\mu_0 [a_e + 2(f+d)l_g + \pi l_g^2]} \quad (7)$$

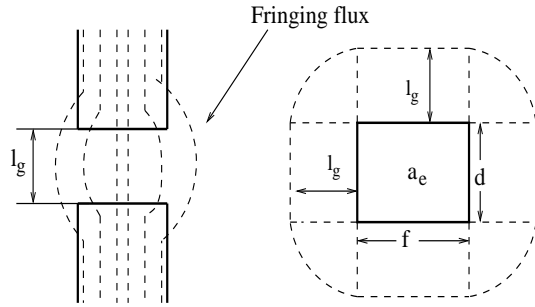


Fig. 2. Effective area considered for calculation

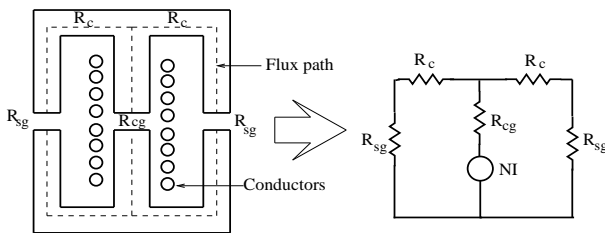


Fig. 3. Magnetic circuit representation of EE core inductor

In the case of EE type of core from Fig 3, there are three possible reluctances: reluctance of the core \mathcal{R}_c , reluctance of the center leg of E core \mathcal{R}_{cg} and reluctance of side leg of E core \mathcal{R}_{sg} . The total reluctance of the magnetic path will be

$$\mathcal{R}_t = \mathcal{R}_{cg} + \frac{\mathcal{R}_{sg}}{2} + \frac{\mathcal{R}_c}{2} \quad (8)$$

(8) is substituted in (3) and (4) to obtain L and B_m as functions of (l_g, N) . Two curves are plotted on a graph of l_g vs N to represent the set of all values of (l_g, N) which give the required L and B_m . The intersection of both curves will give the possible (l_g, N) for which the core will not saturate as well as the required inductance is achieved as shown in Fig 4. The advantage of this numerical method is that as the effect of fringing at the air gap is included in terms of \mathcal{R}_t , the built inductor will have the inductance very close to the initial calculation. The number of possible solutions is also greater which means there is greater flexibility in the actual construction of the inductor.

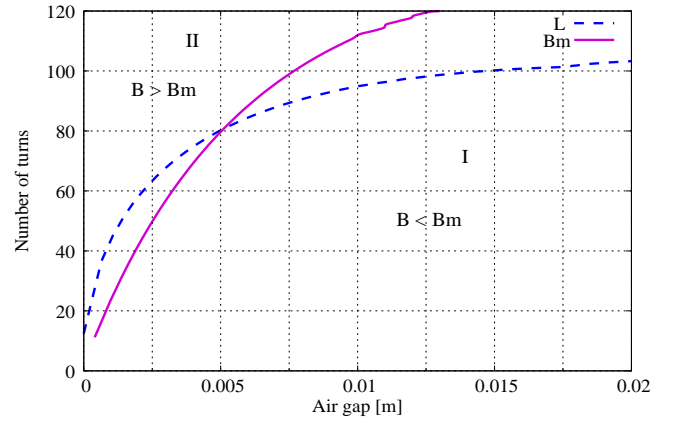


Fig. 4. Intersection of required inductance and flux density limit

From Fig 4, the region II marked by the B_m line represents the design space where the peak flux density exceeds B_m . So all the design points in region II must be avoided to prevent saturation of the core. Region I represents the design space where the peak flux density is less than B_m , so all the possible design points in Region I fulfil the flux density requirements. But there is only one point which also meets the inductance requirement, which is obtained by the intersection of the dashed L line and solid B_m line.

The above graphical analysis assumes that the permeability of the core material is linear for all operating conditions. To further guarantee the accuracy of the final design and to accommodate for variations in manufacturing samples, a minimum air gap is selected such that the air gap reluctance is much larger than the core reluctance. This will minimize the errors due to material and manufacturing tolerances. If the permeability of the core material is dependent on the applied magnetic flux, temperature or other factors, linear magnetic equations cannot be used to accurately determine the inductance. In this case a material characteristic A_L in $\mu\text{H}/(\text{turns})^2$ is usually specified by the manufacturer for

specific core shapes, air gap and flux density. This can be used to accurately determine the inductance of Amorphous and Powder materials.

III. POWER LOSS CALCULATION

A. Core loss

The relationship between H and B in any magnetic material is given by the magnetization curve. The loop area of the magnetization curve represents the energy dissipated per unit volume of the material over a complete magnetization period. The energy loss per cycle can be decomposed into three different components: the frequency independent term W_h (hysteresis loss), the classical loss $W_c \propto f$, and the excess loss $W_e \propto f^{1/2}$ [11]. A detailed evaluation of the core loss requires extensive knowledge of the microstructure of the material along with numerical implementation of mathematical models of hysteresis. However, most manufacturers provide core loss graphs of sufficient accuracy for different frequencies and magnetization levels. The core loss per kg or per cm^3 of a toroidal sample of the magnetic material is plotted as a function of frequency for different magnetic flux densities. From these curves, the core loss P_{co} is expressed as

$$P_{co} = kB_p^x f^y \quad (9)$$

where B_p is the peak magnetic flux density and f is the frequency of the applied current. The factors k , x and y will vary depending on the type of magnetic material and frequency range of operation. The magnetic materials chosen for high frequency operation such as Ferrite, Amorphous, Powder usually have low core loss compared to copper winding loss considering high current high frequency designs. This has been confirmed by experimental observation under steady state operating conditions where temperature rise in the core was less compared to the winding. Hence the core loss graphs published by vendors of magnetic material are sufficient to estimate the core losses.

B. Copper loss

A voltage is induced in a conductor if it is subjected to time varying magnetic flux, according to Faraday's law. The inducing field may be due to its own current, which must be time varying or due to time varying current carried by another adjacent conductor. In the first case the phenomenon is called Skin effect and the second case is called Proximity effect. The induced voltage gives rise to currents distributed throughout the body of the conductor. These two eddy current effects will occur simultaneously in a conductor that carries an alternating current and is positioned in an external alternating field, which is the exact situation of a conductor which is part of the winding of an inductor or transformer. The effect of these eddy currents can be calculated by formulating electromagnetic equations, either in differential form or integral form. The power loss due to these eddy currents is expressed in terms of the AC resistance of the winding R_{ac} . R_{ac} will be more than the ohmic dc resistance of the winding R_{dc} and vary with type

of winding and frequency of applied current. In case of foil conductors [12],

$$R_{ac} = R_{dc} \frac{\Delta}{2} \left[\frac{\sinh 2\Delta + \sin 2\Delta}{\cosh 2\Delta - \cos 2\Delta} + \frac{2(p^2 - 1) \sinh \Delta - \sin \Delta}{3 \cosh \Delta + \cos \Delta} \right] \quad (10)$$

where $\Delta = h_{cu}/\delta$ is defined as the thickness of the winding foil layer h_{cu} normalized to skin depth δ and p is the total number of foil conductor layers in the winding. The skin depth δ is

$$\delta = \sqrt{\frac{2}{\omega \sigma \mu}} \quad (11)$$

where $\omega = 2\pi f$, $\sigma = 58.13 \times 10^6$ S/m (at 25°C) is the conductivity of copper, $\mu = 4\pi \times 10^{-7}$ H/m is the permeability of copper.

In case of round conductors [13],

$$R_{ac} = R_{dc} \frac{\gamma}{2} \left[\frac{\text{ber}\gamma \text{bei}'\gamma - \text{bei}\gamma \text{ber}'\gamma}{\text{ber}^2\gamma + \text{bei}^2\gamma} - 2\pi\eta^2 \left(\frac{4(p^2 - 1)}{3} + 1 \right) \frac{\text{ber}_2\gamma \text{ber}'\gamma + \text{bei}_2\gamma \text{bei}'\gamma}{\text{ber}^2\gamma + \text{bei}^2\gamma} \right] \quad (12)$$

where

$$\gamma = \frac{d_{cu}}{\delta\sqrt{2}} \quad (13)$$

d_{cu} is the diameter of the bare copper wire, δ is the skin depth, η is the porosity factor defined as

$$\eta = \frac{d_{cu}}{d_{tot}} \sqrt{\frac{\pi}{4}} \quad (14)$$

d_{tot} is the total diameter of the copper wire including wire insulation, p is the total number of winding layers, ber and bei are the real and imaginary parts of the modified Bessel function of the first kind. They are defined as

$$\text{ber}\gamma = \text{Re} \left[I_0(\gamma\sqrt{i}) \right] \quad (15)$$

$$\text{bei}\gamma = \text{Im} \left[I_0(\gamma\sqrt{i}) \right] \quad (16)$$

$$\text{ber}'\gamma = \text{Re} \left[\sqrt{i} I_1(\gamma\sqrt{i}) \right] \quad (17)$$

$$\text{bei}'\gamma = \text{Im} \left[\sqrt{i} I_1(\gamma\sqrt{i}) \right] \quad (18)$$

$$\text{ber}_2\gamma = \text{Re} \left[I_2(\gamma\sqrt{i}) \right] \quad (19)$$

$$\text{bei}_2\gamma = \text{Im} \left[I_2(\gamma\sqrt{i}) \right] \quad (20)$$

The AC resistance is calculated separately for different current harmonics. From the AC resistance and rms rating of the current harmonics, the total copper losses can be calculated.

$$P_{cu} = I_1^2 R_{ac(1)} + \dots + I_{sw}^2 R_{ac(sw)} \quad (21)$$

Then the total power loss in the inductor will be given as

$$P_{tot} = P_{co} + P_{cu} \quad (22)$$

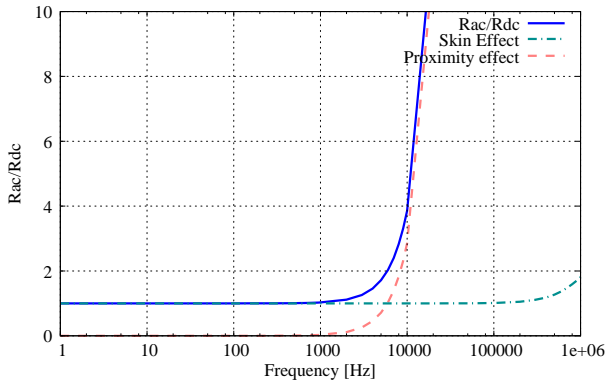


Fig. 5. R_{ac}/R_{dc} for foil winding

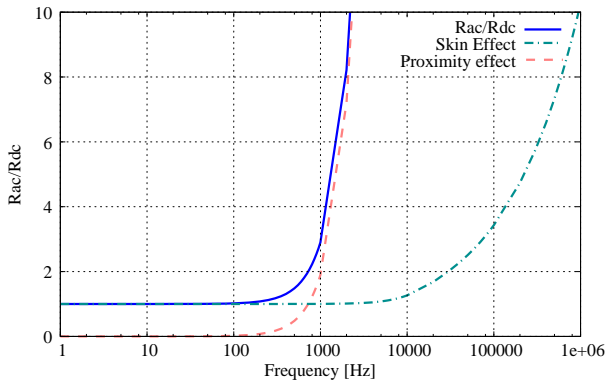


Fig. 6. R_{ac}/R_{dc} for round wire winding

IV. TEMPERATURE RISE ESTIMATION

The principles of heat transfer are used to estimate the surface temperature of the inductor. This is the final step of the inductor design where the entire design procedure is validated on the basis of expected temperature rise. The crucial temperature constraint is the temperature rating of the insulation. The insulation used is Nomex which is rated for 200°C, but filter components are designed to operate at temperature of 100°C.

Heat is transferred from the surface of the inductor by natural convection and/or radiation. In order to solve this heat transfer problem, certain assumptions are made to obtain the simplest model which still yields reasonable results.

- From the thermal analysis point of view, the inductor is considered to be a uniform body with uniform tempera-

TABLE III
PARAMETER LIST FOR R_{ac}/R_{dc} CALCULATION

	Round wire	Foil
Dia / Thickness (mm)	2.643	0.127
Skin depth 50Hz (mm)	9.348	9.348
Skin depth 10kHz (mm)	0.661	0.661
Porosity factor	0.854	*
Turns	120	137
Layers	4	137

ture. This rules out conduction as a mode of heat transfer from the interior to the surface.

- Assuming the room temperature (ie temperature at a point far away from the inductor) to be t_{surr} , the temperature of air immediately surrounding the inductor is assumed to be $t_{surr}+20^\circ\text{C}$.
- The analytical expressions for a natural convection over a simple vertical plate is used to approximate the heat transfer in the inductor. The accuracy of this assumption is verified by experimental measurements of temperature.

When a surface of emissivity ε and surface area A_s at thermodynamic surface temperature T_s is completely enclosed by an much larger surface at a thermodynamic surface temperature T_{surr} separated by a gas (like air) that does not interfere with radiation, the net rate of radiation heat transfer between these two surfaces is given by

$$P_{rad} = \varepsilon\sigma A_s(T_s^4 - T_{surr}^4) \quad (23)$$

In case of convection heat transfer, rate of convection is observed to be proportional to the temperature difference, and is expressed by Newton's law of cooling as

$$P_{conv} = h_{conv}A_s(T_s - T_\infty) \quad (24)$$

where h_{conv} is the convection heat transfer coefficient in $\text{W/m}^2 \text{ }^\circ\text{C}$, A_s is the surface area through which convection heat transfer takes place, T_s is the surface temperature and $T_\infty = t_{surr} + 20^\circ\text{C}$ is the temperature of the fluid sufficiently far away from the surface. From the total power loss in the inductor, the ratio of the convection heat transfer and radiation heat transfer depends on the surface temperature, ambient temperature, and other factors.

$$P_{tot} = P_{conv} + P_{rad} \quad (25)$$

The quantity of interest is the final steady state surface temperature or T_s . But the convection heat transfer coefficient depends on the surface temperature. Hence, T_s is calculated iteratively, by assuming an initial temperature which will give an approximate convection coefficient h_{conv} . Using this h_{conv} and the total heat transfer rate P_{tot} the individual heat transfer rates P_{rad} , P_{conv} and surface temperature T'_s can be found. This T'_s is then used to find new h'_{conv} which is then again used to find the next iteration of T_s . This process is repeated until the surface temperature converges to the expected value [14]. This approach is different from most power electronics designs which directly use the thermal resistance figure R_{th} for estimating the surface temperature. This cannot be used here for two reasons: R_{th} is not specified for the different three-dimensional core geometries and h_{conv} is non-linear and highly sensitive to surface temperature.

- 1) Assume an initial surface temperature T_s .
- 2) For radiation, T_{surr} is assumed to be 25°C (298K) and for natural convection, T_∞ is assumed to be 45°C (318K). Also surface emissivity for radiation is assumed $\varepsilon=0.6$.

3) Calculate the film temperature

$$T_f = \frac{T_s + T_\infty}{2} \quad (26)$$

4) For the film temperature T_f , the properties of air at 1 atm pressure are defined. k is the thermal conductivity of air (W/m K), ν is the kinematic viscosity (m^2/s) and Pr is the Prantl number for air which is tabulated for standard atmospheric pressure at different temperatures [14].

5) The length of the vertical surface is know as the characteristic length L_c . In case of the inductor, this will be equal to the height of the inductor.

6) Calculate the Rayleigh number Ra_L and Nusselt number Nu .

$$Ra_L = \frac{g\beta(T_s - T_\infty)L_c^3 Pr}{\nu^2} \quad (27)$$

$$Nu = \left[0.825 + \frac{0.387 Ra_L^{\frac{1}{4}}}{\left(1 + \left(\frac{0.492}{Pr} \right)^{\frac{9}{16}} \right)^{\frac{8}{27}}} \right]^2 \quad (28)$$

where g is the acceleration due to gravity (9.8m/s^2), β is the volume expansion coefficient $=1/T_s$ and all temperatures are detailed in Kelvin.

7) The convection heat transfer coefficient is given by this equation.

$$h_{conv} = \frac{Nu k}{L_c} \quad (29)$$

8) The net heat transfer rate is equal to the total power dissipated.

$$P_{conv} + P_{rad} = P_{tot} \quad (30)$$

$$P_{tot} = h_{conv} A_s (T_s - T_\infty) + \varepsilon \sigma A_s (T_s^4 - T_{surr}^4) \quad (31)$$

9) Solving this fourth order polynomial equation for T_s gives T'_s . Steps 3-8 are repeated till the surface temperature converges to one number, which will be the actual surface temperature of the inductor for a power loss of P_{tot} .

V. EXPERIMENTAL RESULTS

A. Inductance measurement

Inductance was accurately measured through the impedance frequency response. The high frequency impedance response also indicated the differential mode parasitic impedances. These parasitics are then estimated by fitting the measured frequency response with first and second order transfer functions. The differential mode impedance model of inductors was estimated to be

$$Z_L(s) = (sL + R) \parallel \frac{1}{sC} \quad (32)$$

where L is the designed inductance, R is the resistance of the winding, and C is the parasitic capacitance of the winding. The impedance frequency response was measured

using AP Instruments model 200 ISA analog network analyser. The network analyser has a bandwidth of 15 MHz, at a maximum output of 1.77V. Current measurements were made with Textronix TCP300 AC/DC current probe and amplifier with bandwidth of 120 MHz. The frequency response was measured in the range of 10 Hz to 1 MHz with at least 1000 sampled points, each point internally averaged 40 times by the instrument. The frequency response measurements indicate that the inductor characteristics will not be dominated by the parasitics well above the switching frequency as indicated by Table II.

TABLE IV
INDUCTOR DIFFERENTIAL MODE PARASITICS MEASUREMENT

Core type	L (mH)	C (pF)
Ferrite	3.385	9.6
Amorphous (AMCC 367S)	5.434	3.75
Amorphous (AMCC 630)	5.323	6
Powder (foil winding)	1.737	7.2
Powder (round winding)	1.772	4.9

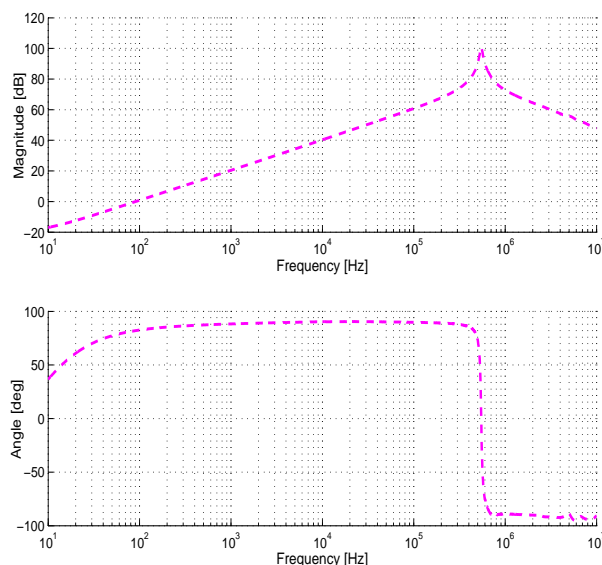


Fig. 7. Differential mode impedance response 10 Hz to 1 MHz; Powder core inductor, foil winding; L=1.73mH, Turns=88

B. Power loss measurement

Table V shows the comparison between measured and calculated power loss. Power measurements were made using a three phase six channel digital power meter. Harmonics were calculated from the current waveform sampled by a digital oscilloscope. For these harmonics, the expected copper and core loss is also calculated. The last row shows the percent error between the measured and expected power loss.

C. Temperature rise measurement

The thermal model from Section IV was verified through DC temperature tests. All the inductors were connected in

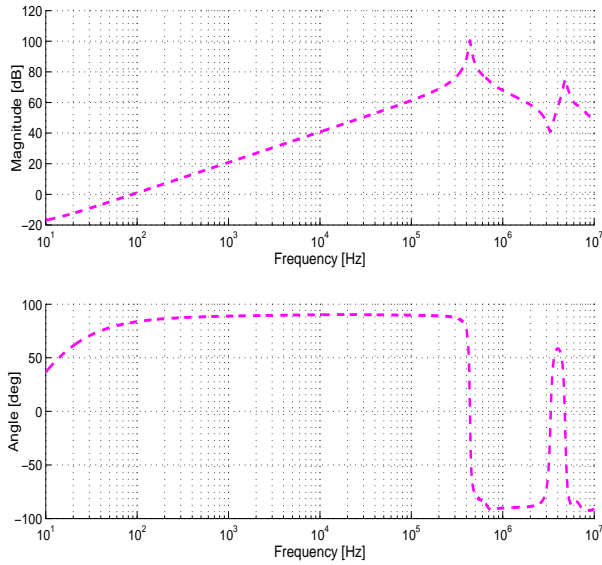


Fig. 8. Differential mode impedance response 10 Hz to 1 MHz; Powder core inductor, round wire winding; $L=1.77\text{mH}$, Turns=90, Layers=4

TABLE V
INDUCTOR POWER LOSS MEASUREMENT

Core type	Expected			Actual Total (W)	Error (%)
	Copper (W)	Core (W)	Total (W)		
Ferrite	27.39	–	27.39	38.6	-29
Amorphous(AMCC 367S)	12.51	6.38	18.89	24	-21.3
Amorphous(AMCC 630)	10.7	6.07	16.77	18.3	-8.3
Powder(foil winding)	13.72	12.92	26.64	35.7	-25.3
Powder(round winding)	36.16	12.94	47.04	35.3	+33.2

series with a adjustable DC current source. Initially current was set at the rated current of the inductor. The temperature of individual inductors was measured using K-type thermocouples embedded inside the winding of the inductor. In most cases, two thermocouples were used per inductor, one embedded close to the first turn (“inner”) and the second at the last turn (“outer”). Concurrently, the electrical power loss in each inductor was accurately measured. When the inductor reached thermal stability the current setting was reduced to a new lower value. Again the temperature was tracked till it became constant. This ensured that precise steady state temperature reading was available for different power levels. The experiment was repeated for decreasing current levels –14 A, 10 A, 7.5 A, 5 A and 2.5 A. It can be seen from Table VI that the actual inductor design is conservative, since the actual surface temperature does not exceed 100°C . Further, the error in analysis vs actual measurement is larger in designs where the core winding window is not fully utilized.

VI. CONCLUSION

This paper presents a simplified and comprehensive approach to inductor design especially for high current, high frequency applications. An iterative design procedure is proposed which does not require a pre-determined core database.

TABLE VI
INDUCTOR TEMPERATURE MEASUREMENT FOR AMBIENT 30°C

Core type	Power loss (W)	Expected rise ($^{\circ}\text{C}$)	Actual rise ($^{\circ}\text{C}$)	Error %
Ferrite	38.8	66	58	13.8
Amorphous (AMCC 367S)	13.52	42	27	55.5
Amorphous (AMCC 630)	9.01	34	20	70
Powder (foil winding)	13.13	44	41	7.3
Powder (round winding)	13.32	47	41	14.6

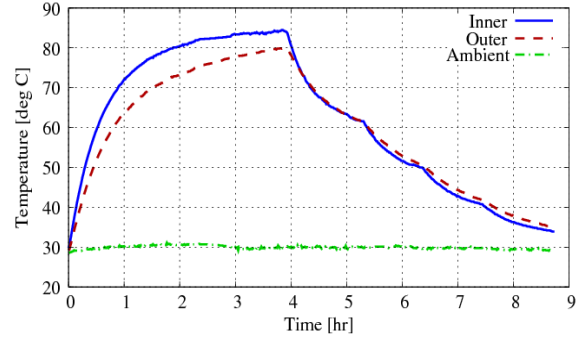


Fig. 9. DC temperature test; Ferrite core inductor with round wire winding

The design parameters which affect the efficiency are analysed and modelled using simplified equations. The area product approach is modified to simplify the design steps and increase the design choices. A novel empirical model for fringing is used to model air gap reluctances. The power loss equations for core and copper are elaborated. The surface temperature of the inductor is modelled with reasonable accuracy for the case of natural convection using principles of heat transfer. Measurements confirm the validity of the design assumptions.

ACKNOWLEDGMENT

The authors would like to thank National Mission for Power Electronics Technology (NaMPET), a national mission program under Ministry of Communications and Information Technology, Government of India for funding this project.

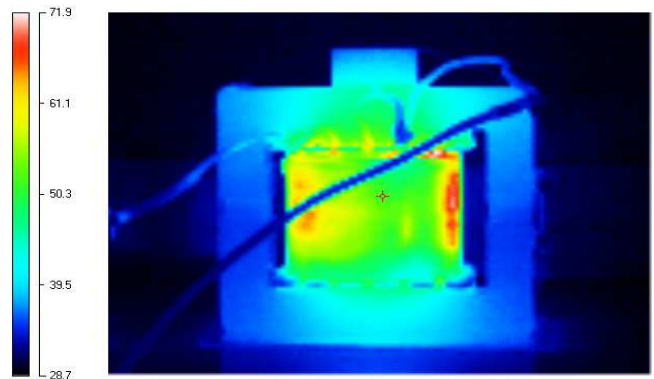


Fig. 10. Thermal image of Ferrite inductor showing winding hotter than core

REFERENCES

- [1] N.Mohan, T.M.Undeland, W.P.Robbins, "Design of magnetic components," in *Power Electronics- Converters, Applications and Design*, 3rd ed., John Wiley and Sons, 2003, pp. 744-792.
- [2] A. van den Bossche, V.Valchev, *Inductors and Transformers for Power Electronics*, 1st ed., Taylor and Francis, 2005
- [3] H.Skarrie, "Design of Powder core inductors," Ph.D. dissertation, Dept. of Ind. Elec. Eng. and Auto., Lund Univ., Lund, Sweden, 2001
- [4] G.S.Ramana Murthy, "Design of Transformers and Inductors at Power-Frequency- A modified Area-Product method," M.Sc(Engineering) Thesis, Indian Institute of Science, March 1999.
- [5] Parikshith B.C, V. John, "Higher order output filter design for grid connected power converters," in National Power Systems Conference (NPSC), IIT Bombay, Dec. 2008, pp. 614-619 [Online]. Available: <http://eprints.iisc.ernet.in/17712/1/p221.pdf>
- [6] Col.Wm.T. McLyman, "AC Inductor Design," in *Transformer and Inductor Design Handbook*, 3rd ed., Marcel Dekker, 2004, pp. 10-1-10-13
- [7] T.G.Wilson, A.Balakrishnan, W.T.Joines, "Air-gap reluctance and inductance calculations for magnetic circuits using a Schwarz-Christoffel transformation," IEEE Trans. on Power Electronics, vol. 12, no. 4, pp. 654-663, July 1997
- [8] A. van den Bossche, V.Valchev, T.Filchev, "Improved approximation for fringing permeances in gapped inductors," *Industry Applications Conference, 2002. 37th IAS Annual Meeting Conference Record of the*, 2002, vol.2, pp. 932- 938
- [9] A.M.Tuckey, D.J.Patterson, "A minimum loss inductor design for an actively clamped resonant DC link inverter," *Proceedings of World Congress on Industrial Applications of Electrical Energy and 35th IEEE- IAS Annual Meeting*, 2000, vol. 5, pp. 3119-3126
- [10] M.Sippola, R.E.Sepponen, "Accurate prediction of high frequency power transformer losses and temperature rise," IEEE Trans. on Power Electronics, vol. 17, no. 5, pp. 835-847, Sept 2002
- [11] G.Bertotti, I.Mayergoyz, *The Science of Hysteresis*, vol. 1,3, Elsevier Inc, 2005
- [12] W.G.Hurley, E.Gath, J.G.Breslin, "Optimizing the AC resistance of multilayer transformer windings with arbitrary current waveforms," IEEE Trans. on Power Electronics, vol. 15, no. 2, pp. 369-376, March 2000
- [13] M.Bartoli, A.Reatti, M.K.Kazimierczuk. (1995, Dec). Modeling winding losses in high frequency power inductors. *J. Circuits, Systems and Computers*, vol.5, no.4, pp. 607-626
- [14] Y.A.Cengel, *Heat and Mass Transfer - A practical approach* (3rd ed.), Tata McGraw Hill, 2007
- [15] A.V.Bossche, V.Valchev, J.Melkebeek, "Thermal modeling of E-type magnetic components," *Proceedings of the 2002 28th Annual Conference of the IEEE Industrial Electronics Society*, 2002, vol. 2, pp. 1312-1317



Amith Gururaj Karanth received his B.E (Electronics and Communications Engineering) degree in 2008 from Visvesvaraya Technological University, Belgaum, India. Subsequently, he worked for over a year and half as a Project Assistant in Power Electronics Group in the Department of Electrical Engineering at the Indian Institute of Science, Bangalore, India. He is currently pursuing his M.Sc (Engineering) degree in Electrical Power Engineering at the Technische Universität Darmstadt, Germany.

His research interests include renewable and sustainable energy technology and power electronics.



Dr. Vinod John received B.Tech. degree in Electrical Engineering from the Indian Institute of Technology, Madras, M.S.E.E. degree from the University of Minnesota, Minneapolis, and Ph.D. from the University of Wisconsin, Madison. He has worked in research and development positions at GE Global Research, Niskayuna, NY and Northern Power, VT. He is currently working as an Assistant Professor at the Indian Institute of Science, Bangalore.

His primary areas of interests are in power electronics and distributed generation, power quality, high power converters and motor drives.



Parikshith B.C received B.E degree in Electrical and Electronic Engineering from Visvesvaraya Technological University, Belgaum, India in 2006 and M.Sc (Engineering) degree in Electrical Engineering from Indian Institute of Science, Bangalore, India in 2010.

His research interests include renewable energy, distributed generation, magnetic components and power quality.